Editors' Suggestion

Superconductivity beyond the Conventional Pauli Limit in High-Pressure $CeSb_2$

Oliver P. Squire, Stephen A. Hodgson, Jiasheng Chen, Vitaly Fedoseev,[†] Christian K. de Podesta, Theodore I. Weinberger, Patricia L. Alireza, and F. Malte Grosche[*]
Cavendish Laboratory, University of Cambridge, Cambridge CB3 0HE, United Kingdom

(Received 1 November 2022; revised 1 May 2023; accepted 31 May 2023; published 10 July 2023)

We report the discovery of superconductivity at a pressure-induced magnetic quantum phase transition in the Kondo lattice system $CeSb_2$, sustained up to magnetic fields that exceed the conventional Pauli limit eightfold. Like $CeRh_2As_2$, $CeSb_2$ is locally noncentrosymmetric around the Ce site, but the evolution of critical fields and normal state properties as $CeSb_2$ is tuned through the quantum phase transition motivates a fundamentally different explanation for its resilience to applied field.

DOI: 10.1103/PhysRevLett.131.026001

In an increasing number of materials—notably the new unconventional superconductors $CeRh_2As_2$ [1] and UTe_2 [2,3]—superconductivity is surprisingly resilient to magnetic field, and the temperature dependence of the upper critical field shows a rich and unexpected structure. This is important not just for applications in which high magnetic fields are required, but also because the field resilience suggests unconventional Cooper pair states, which may be exploited for quantum computing. In $CeRh_2As_2$, the postulated high field state has been linked to a structural peculiarity, namely, the lack of inversion symmetry around the crucially important Ce atoms, which underpin the electronic structure and the superconducting pairing mechanism.

In the related clean Kondo lattice material $CeSb_2$, we here report the discovery of superconductivity over a narrow pressure range that envelops a magnetic quantum critical point (QCP). $CeSb_2$ displays a complex magnetic phase diagram with at least four magnetic phases and a ferromagnetic ground state [4–8], all of which are initially robust under pressure, but its electronic and magnetic properties change profoundly [9,10] at the high pressures considered here. Like $CeRh_2As_2$, high-pressure $CeSb_2$ lacks inversion symmetry around the Ce sites, and its upper critical field is strongly enhanced over expectations from elementary theory. In contrast to $CeRh_2As_2$, however, signatures of an even-parity to odd-parity transition under applied field are not observed in $CeSb_2$, suggesting that the critical field is instead boosted by a more general mechanism intrinsic to strong-coupling superconductivity involving ultraheavy quasiparticles.

Methods.—High-quality crystals of $CeSb_2$ with residual resistivity ratios $RRR = \rho_{300}/\rho_0 \simeq 100$ were grown using standard self-flux techniques [5] and characterized by powder x-ray diffraction, resistivity (see Supplemental Material [11]), magnetization, and heat capacity measurements. Piston-cylinder pressure cell measurements up to about 28 kbar were carried out in a compound BeCu/MP35 cell [18] with the superconducting transition temperature of Sn as the pressure gauge [19], whereas a wider pressure

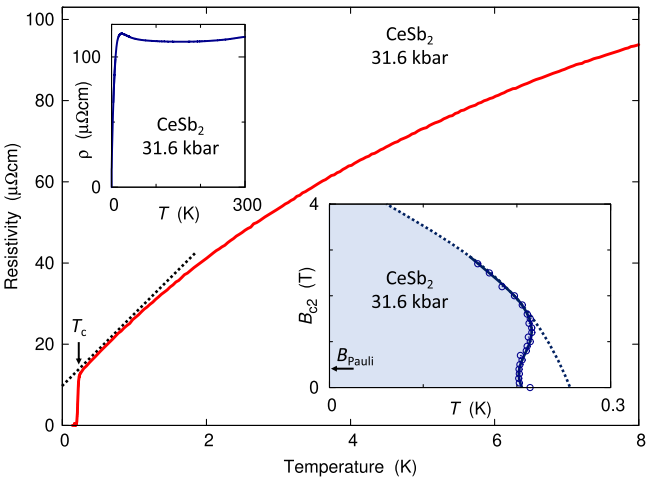

FIG. 1. Superconductivity and anomalous normal state in high-pressure $CeSb_2$. The variation of the resistivity ρ with temperature T shows negative curvature all the way down to a sharp transition to $\rho = 0$ at $T_c \simeq 0.22$ K. Left inset: $\rho(T)$ rises sharply to a shoulder at ~10 K, reaches a shallow maximum at 22.5 K, and then saturates, following a form typical for a Kondo lattice with a low effective bandwidth. Right inset: the resistive upper critical field follows an inverted S shape at low fields $\|c$. At intermediate fields, it takes on a large negative slope, which would extend to higher T_c (dashed line) without the S anomaly. It far exceeds the Pauli paramagnetic limit $B_{\mathrm{Pauli}} \simeq 1.84\ \mathrm{T\,K^{-1}}\ T_c(B = 0)$ (horizontal arrow).

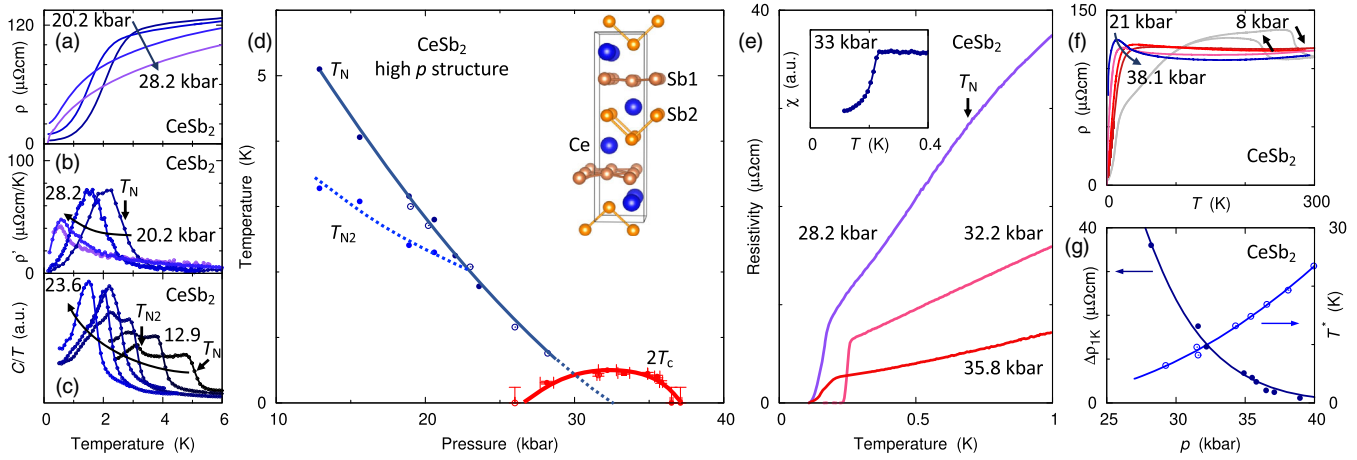

FIG. 2. Pressure dependence of magnetic and superconducting states in high-pressure $CeSb_2$. (a)–(c) Transition anomalies: (a) kink in $\rho(T)$, (b) associated jump in $\rho' = d\rho/dT$, (c) jumps in the heat capacity Sommerfeld ratio C/T. The $\rho(T)$ and $\rho'(T)$ data cover pressures from 20.2 to 28.2 kbar, above which these transition anomalies were no longer resolved. The heat capacity was measured at pressures ranging from 12.9 to 23.6 kbar. It shows a second transition anomaly at a lower temperature T_{N2}, in line with μSR data [17], which indicates that the low-T state is magnetically ordered. (d) High-pressure phase diagram of $CeSb_2$, showing the gradual suppression of the two magnetic transitions [full circles, from $C(T)$; empty circles, from $\rho(T)$] and a superconducting dome [full and empty symbols from $\rho(T)$ in two different samples, square: from magnetic susceptibility χ as in the inset to (e)]. (e) $\rho(T)$ at different pressures straddling the QCP, showing the peak T_c at $p_c \simeq 32$ kbar, where a magnetic transition (arrow in 28.2 kbar data) extrapolates to zero, the quasilinear form of $\rho(T)$ at p_c, and the rapid suppression of $\rho(T)$ at low T with increasing pressure. Inset to (e): high-p susceptibility data showing the superconducting transition. (f) Normal state resistivity up to room temperature, showing the hysteretic signature of the high-T structural transition at 8 kbar (arrows for cooling and warming data) and the very different form of $\rho(T)$ at higher pressures, typical for a Kondo lattice with a low characteristic temperature T^*. We estimate T^* from the shoulder in $\rho(T)$, at which $\rho(T)$ reaches 80% of $\max(\rho)$. (g) Pressure dependence of T^* and of the resistivity increment $\Delta\rho_{1K} = \rho(1\mathrm{K}) - \rho_0$, showing the rapid reduction of the T dependence of $\rho(T)$ at low T and the concomitant increase of T^* with p.

range was accessed in moissanite anvil cells using room temperature ruby fluorescence to determine the pressure. Glycerol was used as the pressure medium. The crystal orientation reported in magnetic field studies (c axis vs in plane) refers to the low-pressure structure. The electrical resistivity was determined using a standard four-terminal ac technique with a 3 μA current at the lowest temperatures, and the magnetic susceptibility was measured using a mutual inductance technique with a pickup microcoil inside the high-pressure sample volume [20]. The heat capacity was obtained from a 3ω temperature modulation technique [11]. Measurements in a Quantum Design PPMS in the range 2–300 K were complemented by low-temperature studies in a cryogen-free adiabatic demagnetization refrigerator (Dryogenic) to < 0.1 K and in fields of up to 6 T.

Superconductivity and anomalous normal state.—The normal state in-plane resistivity in $CeSb_2$ at an applied pressure $p \simeq 31.6$ kbar displays a distinctly non-Fermi liquid, sublinear temperature dependence $\rho(T)$ at low T (Fig. 1 main panel). The resistivity rises steeply and reaches a shallow maximum at 22.5 K, above which it stays roughly constant up to room temperature (left inset in Fig. 1). It follows a form familiar from other Ce- or Yb-based Kondo lattice materials such as $CeCu_2Si_2$, $CeCoIn_5$, and $YbRh_2Si_2$ [21–24], suggesting extremely strong electronic correlations, narrow renormalized bands, and high quasiparticle masses in high-pressure $CeSb_2$.

A sharp resistive transition with midpoint $T_c \simeq 0.22$ K (main plot in Fig. 1) indicates superconductivity at very low temperatures, in line with the low electronic energy scales suggested by the normal state $\rho(T)$. Superconductivity proves surprisingly robust to applied magnetic fields along the crystallographic c direction (right inset in Fig. 1). It persists to > 3 T at low T, exceeding the Pauli paramagnetic limiting field, which is conventionally written as $B_{\mathrm{Pauli}} = 1.84\ \mathrm{T\,K^{-1}}\,T_c$ [25,26], by nearly an order of magnitude. The in-plane upper critical field is similarly enhanced (see Supplemental Material [11]).

For small applied fields, T_c is initially reduced, then rises again to a value slightly higher than the zero-field T_c, for $B \simeq 1.5$ T (right inset of Fig. 1). This produces an unusual, inverted S-shaped structure in the $B_{c2}(T)$ curve. The inverted S structure is observed at several other pressures ≤ 32.2 kbar but vanishes at higher pressures (see below). The sign reversal of dB_{c2}/dT, which is > 0 over an intermediate field range, points toward an underlying field tuned phase transition within the normal state [11].

Quantum critical point.—Distinct transition anomalies are indeed observed at pressures less than $p_c \simeq 32$ kbar [Figs. 2(a)–2(c)]. Electric transport measurements for $p < p_c$ find a kink in $\rho(T)$ at low T, which causes a jump

in the T derivative of the resistivity $\rho'(T)$ [Figs. 2(a) and 2(b)]. Heat capacity measurements under pressure likewise display a jump in $C(T)$ [Fig. 2(c)] at a transition temperature T_N, which agrees with that of the kink in $\rho(T)$. T_N extrapolates to zero temperature at p_c [Fig. 2(d)], indicating a quantum phase transition and, if the transition remains continuous, a quantum critical point. The steplike signatures in C and ρ' at T_N, the gradual p dependence of T_N, and the non-Fermi liquid form of $\rho(T)$ near p_c are all consistent with the transition at T_N being continuous and with our identification of a QCP at p_c. Heat capacity data furthermore show evidence for a weaker second transition at a lower temperature T_{N2}, which merges with T_N as pressure is increased. High-pressure muon spin rotation studies indicate two distinct magnetically ordered states associated with T_N and T_{N2} [17], which is reminiscent of the $CeCu_2(Si/Ge)_2$ system [27] and of $YbRh_2Si_2$ under pressure [24]. The superconducting transition has likewise been tracked in high-pressure transport measurements using two anvil cells and a susceptibility measurement in a third anvil cell [inset of Fig. 2(e)]. Superconductivity is seen to be tightly confined to the immediate vicinity of the magnetic quantum critical point [Fig. 2(d)], indicating a prominent role for magnetic fluctuations in the superconducting pairing mechanism.

Normal and superconducting properties of $CeSb_2$ evolve rapidly with pressure [Figs. 2(e)–2(g)]. The low-T resistivity takes a quasilinear T dependence near p_c [Fig. 2(e)], which saturates to a nearly constant resistivity [Fig. 2(f)] above a low $T^* \sim 10$ K. The low-T slope of $\rho(T)$, measured by the resistivity increment $\Delta\rho_{1K} = \rho(1K) - \rho_0$ over the extrapolated residual resistivity ρ_0, diminishes rapidly with increasing pressure. This is accompanied by a steep increase in T^*, demonstrating that compression under applied pressure strongly increases the effective electronic bandwidth in $CeSb_2$ [Fig. 2(g)].

High-pressure structure.—$CeSb_2$ forms in the orthorhombic $SmSb_2$ structure (space group 64), which lacks inversion symmetry around the Ce site but is centrosymmetric around the center of the unit cell. Transport measurements at intermediate pressures $6\,\text{kbar} < p < 17\,\text{kbar}$ show a highly hysteretic resistivity anomaly [e.g., 8 kbar data in Fig. 2(f)], which shifts to lower temperature with increasing pressure [9] and disappears beyond 17 kbar, where the low-T state differs profoundly from the low-T state at ambient pressure [10]. High-pressure x-ray diffraction [17] has established that this anomaly signals a first-order structural phase transition, which at low T is complete by about 17 kbar. The superconducting and magnetic states discussed above are therefore all associated with the high-pressure structure of $CeSb_2$. The rare earth (R) diantimonides RSb_2 adopt a variety of structure types, all of which lack inversion symmetry around the rare earth site: $SmSb_2$ (like $CeSb_2$ at $p = 0$), $HoSb_2$ (orthorhombic, space group 21), $EuSb_2$ (monoclinic, space group 11), and $YbSb_2$ (orthorhombic, space group 63). The x-ray data and *ab initio* calculations [17] unambiguously rule out the $SmSb_2$ and $HoSb_2$ structures for high-pressure $CeSb_2$ and favor the $YbSb_2$ structure [inset in Fig. 2(d)]. Pronounced magnetoresistance anisotropy (see Supplemental Material [11]) suggests that samples retain their crystallinity when changing into the high-pressure structure under applied pressure.

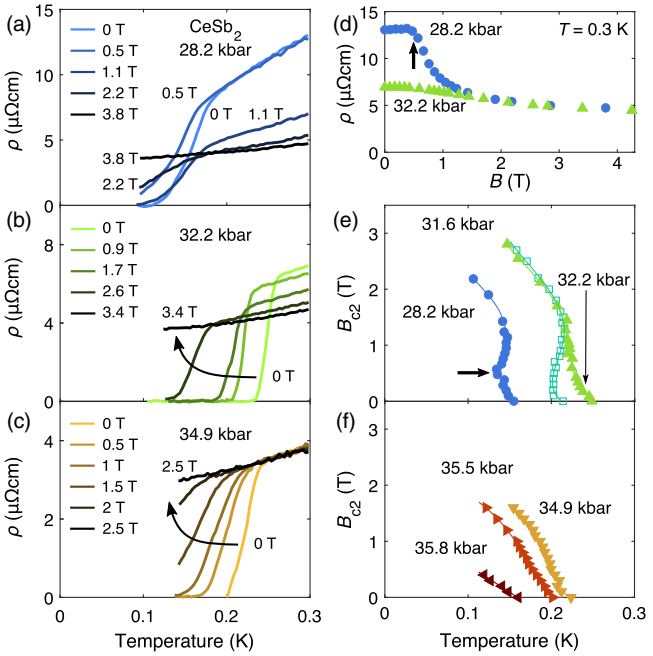

FIG. 3. (a)–(c) Response of the superconducting transition in $CeSb_2$ to magnetic field applied along the c axis as defined for the low-p structure, (a) for $p < p_c$, (b) for $p \simeq p_c$, and (c) for $p > p_c$. (d) The magnetoresistance at $T > T_c$ displays a distinct kink at $\simeq$0.5 T (vertical arrow) for $p < p_c$, indicating a field-induced transition out of the magnetically ordered state. (e) $B_{c2}(T)$ curves extracted from the midpoint of the resistive transition display a pronounced inverted S shape with a local minimum of T_c at $\simeq$0.5 T for $p = 28.2$ kbar (horizontal arrow), which corresponds to the kink field in (d). (f) At $p > p_c$ the $B_{c2}(T)$ curves revert to a more conventional form.

Critical fields.—The locally noncentrosymmetric structure of high-pressure $CeSb_2$ invites comparison to $CeRh_2As_2$ [1,28–32] and other unconventional superconductors such as UTe_2, UGe_2, and UPt_3 (e.g., [33]) when considering the response to applied magnetic field. Both the form of the critical field curve $B_{c2}(T)$ in $CeSb_2$ and the magnitude of the upper critical field are unusual. We consider first the inverted S-shaped form for $B_{c2}(T)$ displayed in the inset of Fig. 1. The initial reduction, then increase of T_c with field is most pronounced at the lowest pressure at which full resistive transitions could be observed [28.2 kbar, Fig. 3(a)]. It is already weaker at 31.6 kbar (Fig. 1) and weaker still close to the QCP, at 32.2 kbar [Figs. 3(b) and 3(e)]. Comparing $B_{c2}(T)$ at these last two pressures [Fig. 3(e)] shows that, near the QCP, the

critical field curves converge on a single line at high fields but differ at low fields. At pressures above p_c, the critical field curves gradually change into the conventional form [Fig. 3(f)]. The relative reduction of T_c at low fields < 0.5 T for $p < p_c$ could be seen as a signature of a field-induced transition between two distinct superconducting states, as in $CeRh_2As_2$ [1], or it might result from a field-induced magnetic transition. The steplike magnetoresistance anomaly at 28.2 kbar shown in Fig. 3(d) points toward the second scenario. The transition field of $\simeq 0.5$ T (vertical arrow) corresponds to the minimum T_c in the 28.2 kbar critical field curve in Fig. 3(e) (horizontal arrow). These findings suggest that the inverted S shape of $B_{c2}(T)$ on the ordered side of the QCP results from the interplay between applied field and the magnetic spin fluctuation spectrum: tuning the system out of the magnetically ordered state with increasing field enhances order parameter fluctuations and the associated pairing interaction, thereby strengthening superconductivity. A similar explanation has been advanced in pressurized UGe_2 [34].

Considering next the eightfold enhancement of B_{c2} over the conventional Pauli limit $B_{\mathrm{Pauli}} = 1.84\ \mathrm{T\,K^{-1}}T_c$ [25,26] in $CeSb_2$, we note that moderate violations of the Pauli limit are common in Ce-based heavy fermion materials such as $CeCoIn_5$ and $CeCu_2Si_2$ (Table I) without necessarily being taken as evidence for triplet pairing. The ratio of the high initial slope B'_{c2} over T_c in compressed $CeSb_2$ indicates a very high Sommerfeld ratio $C/T \sim 1.2\ \mathrm{J/molK^2}$ (Table I) (see Supplemental Material [11]). It is larger than the corresponding ratios in UPt_3, $CeCoIn_5$, $CeCu_2Si_2$, and UBe_{13}, suggesting that the quasiparticles underlying superconductivity in high-pressure $CeSb_2$ are among the heaviest ever recorded in a superconducting heavy fermion material. This is significant, because theoretical studies [35,36] indicate that violations of Pauli limiting may generally be expected in superconductors with large mass renormalization, irrespective of whether the pairing is mediated by phonons or spin fluctuations and whether the pairing state has s-wave or d-wave symmetry [37]. The original calculation of the conventional Pauli limiting field [26,38] balances the superconducting condensation energy against the magnetic energy involved in changing the spin alignment of the paired electrons in an applied field. The former depends on the energy gap, the latter on the spin susceptibility. Although some uncertainty in the latter arises from imprecise knowledge of the conduction electron g factor, this would have to be $\ll 1$ to explain substantially enhanced Pauli limiting fields, which is difficult to justify: strong anisotropy of the g factor is ruled out by the similarly large B_{c2} observed for $B \perp c$ [11]. In strong-coupling superconductors, the balance between condensation energy and magnetic energy needs to be modified both on the side of the condensation energy, because the energy gap may be far larger than the Bardeen-Cooper-Schrieffer relation $\Delta = 1.76 k_B T_c$ suggests, and on the side of the magnetic energy, because the spin susceptibility is reduced below the Pauli susceptibility indicated by the quasiparticle density of states by as much as the interaction-induced mass enhancement. In model calculations, this causes the Pauli limit to be boosted to about $1.5\ \mathrm{T\,K^{-1}}T_c m^*/m_b$, where m^* is the renormalized quasiparticle mass and m_b is the bare band mass [35]. In UBe_{13}, the eightfold enhancement of B_{c2} over the conventional Pauli limit (Table I) has been interpreted likewise [46] in terms of a strong-coupling calculation, and a similar boost to the limiting field was found in a calculation for spin-fluctuation-induced d-wave pairing [37]. In this approach, resilience to high fields is accompanied by increasing admixture of a frequency-odd triplet pairing state into the underlying frequency-even singlet pairing state [39,40] (see also [41,42] for material-specific calculations). This general route contrasts starkly with the scenario advanced for $CeRh_2As_2$ (e.g., [1]), which is predicated on its locally noncentrosymmetric structure. In heavy fermion materials such as $CeSb_2$, a quantitative calculation is hindered by the similar magnitudes of the Zeeman energy at B_{c2} and electronic as well as bosonic energy scales, by the effect of the applied field on the pairing interaction, by the highly anomalous normal state, which deviates profoundly from expectations of Fermi liquid theory, and by our incomplete understanding of the origins of mass renormalization and

TABLE I. Critical field data for selected heavy fermion superconductors. T_c, initial slope of the upper critical field B'_{c2}, experimental B_{c2} in the low-T limit, and C/T at T_c have been extracted from the literature. The Pauli limit B_{Pauli} is calculated as $1.84\ \mathrm{T\,K^{-1}}T_c$. Elementary theory predicts that $\sqrt{B'_{c2}/T_c} \propto C/T$ [11], as is indeed roughly confirmed by the tabulated data. Applying this analysis to $CeSb_2$ near p_c, at 34.9 kbar, produces an estimate for C/T of $\sim 1.2\ \mathrm{J/molK^2}$.

	T_c (K)	B'_{c2} (T/K)	B_{Pauli} (T)	$B_{c2}(0)$ (T)	$\sqrt{B'_{c2}/T_c}$ ($\mathrm{T^{1/2}/K}$)	C/T ($\mathrm{J/molK^2}$)
$CeCoIn_5$ [43]	2.2	30.5	4.05	11.5	3.7	0.3
$CeCu_2Si_2$ [44]	0.6	35	1.10	1.9	7.6	0.7
$CeRh_2As_2$ [1]	0.26	97	0.48	14	19.3	2
$CeSb_2$ ($\simeq p_c$)	0.22	30	0.40	>3	11.8	1.2 (est.)
UPt_3 [45]	0.52	6.3	0.96	1.8	3.5	0.4
UBe_{13} [46]	0.95	45	1.75	14	6.9	1

pairing interaction, which do not align completely. The intriguing suggestion that increasing admixture of odd-frequency triplet superconductivity may boost the critical field in strongly correlated materials should be tested in more detailed theoretical and computational investigations.

Conclusions.—High-pressure $CeSb_2$ emerges as a clean, ultraheavy fermion system with superconductivity forming out of a pronounced non-Fermi liquid state and an upper critical field far beyond the Pauli limit. Because the QCP underlying the superconducting dome can in $CeSb_2$ be crossed under pressure, this material supplies an excellent test case for refining our understanding of unconventional superconductivity. Our findings suggest that strong mass renormalization boosts the magnitude of B_{c2} without an even-parity to odd-parity phase transition as reported in $CeRh_2As_2$, and that the interplay between applied field, magnetic order, and the associated magnetic fluctuations can explain the evolution of $B_{c2}(T)$ across the QCP.

All data needed to evaluate the conclusions in the paper are present in the paper, the Supplementary Materials, and the Data Repository at the University of Cambridge and can be downloaded from [47].

We thank, in particular, A. Chubukov, R. Tao, and G. Lonzarich for helpful discussions and Z. Feng and Y. Zou for early work on the structural and magnetic transitions in $CeSb_2$. The project was supported by the EPSRC of the UK (Grants No. EP/K012894 and No. EP/P023290/1) and by Trinity College.

*fmg12@cam.ac.uk
†Present address: Department of Physics, Massachusetts Institute of Technology, Cambridge, Massachusetts 02139, USA.

[1] S. Khim, J. Landaeta, J. Banda, N. Bannor, M. Brando, P. Brydon, D. Hafner, R. Küchler, R. Cardoso-Gil, U. Stockert, A. P. Mackenzie, D. F. Agterberg, C. Geibel, and E. Hassinger, Science **373**, 1012 (2021).
[2] S. Ran, C. Eckberg, Q.-P. Ding, Y. Furukawa, T. Metz, S. R. Saha, I.-L. Liu, M. Zic, H. Kim, J. Paglione, and N. P. Butch, Science **365**, 684 (2019).
[3] D. Aoki, A. Nakamura, F. Honda, D. Li, Y. Homma, Y. Shimizu, Y. J. Sato, G. Knebel, J.-P. Brison, A. Pourret, D. Braithwaite, G. Lapertot, Q. Niu, M. Vališka, H. Harima, and J. Flouquet, J. Phys. Soc. Jpn. **88**, 043702 (2019).
[4] P. C. Canfield, J. D. Thompson, and Z. Fisk, J. Appl. Phys. **70**, 5992 (1991).
[5] S. L. Bud'ko, P. C. Canfield, C. H. Mielke, and A. H. Lacerda, Phys. Rev. B **57**, 13624 (1998).
[6] Y. Zhang, X. Zhu, B. Hu, S. Tan, D. Xie, W. Feng, L. Qin, W. Zhang, Y. Liu, H. Song, L. Luo, Z. Zhang, and X. Lai, Chin. Phys. B **26**, 067102 (2017).
[7] B. Liu, L. Wang, I. Radelytskyi, Y. Zhang, M. Meven, H. Deng, F. Zhu, Y. Su, X. Zhu, S. Tan, and A. Schneidewind, J. Phys. Condens. Matter **32**, 405605 (2020).
[8] C. Trainer, C. Abel, S. L. Bud'ko, P. C. Canfield, and P. Wahl, Phys. Rev. B **104**, 205134 (2021).
[9] T. Kagayama, G. Oomi, S. Bud'ko, and P. Canfield, Physica (Amsterdam) **281B**, 90 (2000).
[10] T. Kagayama, Y. Uwatoko, S. Bud'ko, and P. Canfield, Physica (Amsterdam) **359–361B**, 320 (2005).
[11] See Supplemental Material at http://link.aps.org/supplemental/10.1103/PhysRevLett.131.026001, for further details of the in-plane critical field, an assessment of crystallinity across the structural transition, estimates based on the critical field data, implications of the sign-reversal of $B'_{c2}(T)$, the temperature modulation heat capacity method, and ambient pressure resistivity data supporting the RRR estimate, which includes Refs. [12–16].
[12] E. Helfand and N. R. Werthamer, Phys. Rev. **147**, 288 (1966).
[13] M. Tinkham, *Introduction to Superconductivity* (Dover Publications, New York, 2004).
[14] T. P. Orlando, E. J. McNiff, S. Foner, and M. R. Beasley, Phys. Rev. B **19**, 4545 (1979).
[15] P. F. Sullivan and G. Seidel, Phys. Rev. **173**, 679 (1968).
[16] E. Gati, G. Drachuck, L. Xiang, L.-L. Wang, S. L. Bud'ko, and P. C. Canfield, Rev. Sci. Instrum. **90**, 023911 (2019).
[17] C. de Podesta, T. Weinberger, O. Squire, Z. Feng, J. Chen, G. I. Lampronti, R. Khasanov, and F. M. Grosche (unpublished).
[18] I. R. Walker, Rev. Sci. Instrum. **70**, 3402 (1999).
[19] T. Smith, C. Chu, and M. Maple, Cryogenics **9**, 53 (1969).
[20] P. L. Alireza and S. R. Julian, Rev. Sci. Instrum. **74**, 4728 (2003).
[21] B. Bellarbi, A. Benoit, D. Jaccard, J. M. Mignot, and H. F. Braun, Phys. Rev. B **30**, 1182 (1984).
[22] C. Petrovic, P. G. Pagliuso, M. F. Hundley, R. Movshovich, J. L. Sarrao, J. D. Thompson, Z. Fisk, and P. Monthoux, J. Phys. Condens. Matter **13**, L337 (2001).
[23] A. Malinowski, M. F. Hundley, C. Capan, F. Ronning, R. Movshovich, N. O. Moreno, J. L. Sarrao, and J. D. Thompson, Phys. Rev. B **72**, 184506 (2005).
[24] O. Trovarelli, C. Geibel, S. Mederle, C. Langhammer, F. M. Grosche, P. Gegenwart, M. Lang, G. Sparn, and F. Steglich, Phys. Rev. Lett. **85**, 626 (2000).
[25] A. M. Clogston, Phys. Rev. Lett. **9**, 266 (1962).
[26] B. S. Chandrasekhar, Appl. Phys. Lett. **1**, 7 (1962).
[27] H. Yuan, F. Grosche, M. Deppe, C. Geibel, G. Sparn, and F. Steglich, Science **302**, 2104 (2003).
[28] D. Möckli and A. Ramires, Phys. Rev. B **104**, 134517 (2021).
[29] J. F. Landaeta, P. Khanenko, D. C. Cavanagh, C. Geibel, S. Khim, S. Mishra, I. Sheikin, P. M. R. Brydon, D. F. Agterberg, M. Brando, and E. Hassinger, Phys. Rev. X **12**, 031001 (2022).
[30] D. C. Cavanagh, T. Shishidou, M. Weinert, P. M. R. Brydon, and D. F. Agterberg, Phys. Rev. B **105**, L020505 (2022).
[31] D. Hafner, P. Khanenko, E.-O. Eljaouhari, R. Küchler, J. Banda, N. Bannor, T. Lühmann, J. F. Landaeta, S. Mishra, I. Sheikin, E. Hassinger, S. Khim, C. Geibel, G. Zwicknagl, and M. Brando, Phys. Rev. X **12**, 011023 (2022).

[32] M. Kibune, S. Kitagawa, K. Kinjo, S. Ogata, M. Manago, T. Taniguchi, K. Ishida, M. Brando, E. Hassinger, H. Rosner, C. Geibel, and S. Khim, Phys. Rev. Lett. **128**, 057002 (2022).
[33] T. Hazra and P. Coleman, Phys. Rev. Lett. **130**, 136002 (2023).
[34] I. Sheikin, A. Huxley, D. Braithwaite, J. P. Brison, S. Watanabe, K. Miyake, and J. Flouquet, Phys. Rev. B **64**, 220503(R) (2001).
[35] M. Schossmann and J. P. Carbotte, Phys. Rev. B **39**, 4210 (1989).
[36] J. P. Carbotte, Rev. Mod. Phys. **62**, 1027 (1990).
[37] A. Pérez-González, Phys. Rev. B **54**, 16053 (1996).
[38] A. M. Clogston, A. C. Gossard, V. Jaccarino, and Y. Yafet, Phys. Rev. Lett. **9**, 262 (1962).
[39] M. Schossmann and E. Schachinger, Phys. Rev. B **33**, 6123 (1986).
[40] M. Matsumoto, M. Koga, and H. Kusunose, J. Phys. Soc. Jpn. **81**, 033702 (2012).
[41] A. Aperis, P. Maldonado, and P. M. Oppeneer, Phys. Rev. B **92**, 054516 (2015).
[42] A. Aperis, E. V. Morooka, and P. M. Oppeneer, Ann. Phys. (Amsterdam) **417**, 168095 (2020).
[43] C. F. Miclea, M. Nicklas, D. Parker, K. Maki, J. L. Sarrao, J. D. Thompson, G. Sparn, and F. Steglich, Phys. Rev. Lett. **96**, 117001 (2006).
[44] S. Kittaka, Y. Aoki, Y. Shimura, T. Sakakibara, S. Seiro, C. Geibel, F. Steglich, Y. Tsutsumi, H. Ikeda, and K. Machida, Phys. Rev. B **94**, 054514 (2016).
[45] J. W. Chen, S. E. Lambert, M. B. Maple, Z. Fisk, J. L. Smith, G. R. Stewart, and J. O. Willis, Phys. Rev. B **30**, 1583 (1984).
[46] F. Thomas, B. Wand, T. Lühmann, P. Gegenwart, G. R. Stewart, F. Steglich, J. P. Brison, A. Buzdin, L. Glémot, and J. Flouquet, J. Low Temp. Phys. **102**, 117 (1996).
[47] 10.17863/CAM.97144.